THE JOURNAL OF BIOLOGICAL CHEMISTRY VOL. 283, NO. 35, pp. 24177–24184, August 29, 2008

Structural Basis for Toxin Resistance of β4-Associated Calcium-activated Potassium (BK) Channels*[S]

Received for publication, January 9, 2008, and in revised form, May 19, 2008 Published, JBC Papers in Press, June 16, 2008, DOI 10.1074/jbc.M800179200

Geliang Gan[‡1], Hong Yi[§1], Maorong Chen[‡], Liang Sun[‡], Wenxin Li[§], Yingliang Wu[§2], and Jiuping Ding[‡3]

From the [‡]Key Laboratory of Molecular Biophysics (Huazhong University of Science and Technology) Ministry of Education, College of Life Science and Technology, Wuhan, Hubei, 430074 and [§]State Key Laboratory of Virology, College of Life Sciences, Wuhan University, Wuhan, Hubei 430072, China

The functional diversity of large conductance Ca^{2+}- and voltage-dependent K^+ (BK) channels arises mainly from co-assembly of the pore-forming mSlo α subunits with four tissue-enriched auxiliary β subunits. The structural basis of the interaction between α subunits with β subunits is not well understood. Using computational and experimental methods, we demonstrated that four mSlo turrets decentralized distally from the channel pore to provide a wide open conformation and that the mSlo and hβ4 subunits together formed a "helmet" containing three basic residues (Lys-120, Arg-121, and Lys-125), which impeded the entry of charybdotoxin (ChTX) by both the electrostatic interaction and limited space. In addition, the tyrosine insert mutant (in100Y) showed 56% inhibition, with a K_d = 17 nM, suggesting that the hβ4 lacks an external ChTX-binding site (Tyr-100). We also found that mSlo had an internal binding site (Tyr-294) in the α subunits that could "permanently" block 15% of mSlo+hβ4 currents in the presence of 100 nM ChTX. These findings provide a better understanding of the diverse interactions between α and β subunits and will improve the design of channel inhibitors.

It is well known that functional diversity of large conductance Ca^{2+}- and voltage-dependent potassium (BK) channels arises mainly from co-expression of the pore-forming α subunits with the tissue-enriched auxiliary β subunits (1–10). Four mammalian β genes (β1–β4) are responsible for a variety of the kinetic and pharmacological characteristics of BK channels in native tissues, even though they share sequence homology. For instance, the brain-enriched hβ4 subunits not only alter the conductance-voltage curve of mSlo channels but also slow both the activation and deactivation time courses, suggesting that β4 plays a critical role in the regulation of neuronal excitability and neurotransmitter release (9). Furthermore, results from experiments with a β4 knock-out showed reduced dentate gyrus excitability and protection against temporal lobe seizures (11).

Natural venomous peptides have been used widely to probe the pore conformation of potassium channels. One particular scorpion toxin, charybdotoxin (ChTX),[4] was used to probe the pore structure of BK channels. It is known that the α+hβ1 has a K_d for ChTX similar to that of mSlo channels (4). However, BK channels associating with the β2 or β3 subunits usually have about 30-fold lower sensitivity to ChTX in equilibrium (3, 4), whereas the α+hβ4 channel has about 1000-fold slower association with the toxin (7). Is there a common mechanism working for all of four β genes?

To explore the toxin resistance mechanism of hβ4 subunits, Jin *et al.* (12) investigated how the *N*-linked glycosylation of the hβ4 subunit modulated the toxin sensitivity of hSlo+hβ4 channels. They confirmed that the double glycosylation site mutated in hβ4 showed reduced protection of the channel against toxin blockade as compared with the hSlo channel co-expressed with the wild type hβ4 subunits. Another study is in regard to the removal of the rectification of BK channels co-expressed with hβ3b subunits (13). The extracellular application of 20 mM dithiothreitol completely removed the outward rectification of α+hβ3b channels and restored the sensitivity of α alone to ChTX. All β subunits of BK channels contain a cysteine-rich extracellular segment linking two transmembrane segments. Dithiothreitol can reduce the disulfide linkages of the outer region of β subunits to restore the sensitivity to toxins. Accordingly, it is necessary to understand why the hβ4 subunit has such low sensitivity to ChTX. In this study, we investigated whether the aromatic and electrostatic interactions between the peptide and BK channel could affect toxin sensitivity, which may help us better understand the various co-assembly pathways of BK channels, and provide clues for optimal peptide design in the future.

EXPERIMENTAL PROCEDURES

Constructs—The full-length cDNAs for mSlo1 and hβ4 were subcloned into pcDNA3.1 Zeo(+) and pIRES2-EGFP (Clontech), respectively. Mutations were created with the QuickChange site-directed mutagenesis kit (Stratagene). All of the constructs were verified by DNA sequencing.

Cell Culture and Transfection—HEK293 cells were cultured in Dulbecco's modified Eagle's medium supplemented with 10% fetal bovine serum and incubated at 37 °C in 5% CO_2. One day before transfection, cells were transferred to 24-well plates.

* This work was supported by National Science Foundation of China Grants 30770522, 30470449, 30530140, and 30770519. The costs of publication of this article were defrayed in part by the payment of page charges. This article must therefore be hereby marked "*advertisement*" in accordance with 18 U.S.C. Section 1734 solely to indicate this fact.

[S] The on-line version of this article (available at http://www.jbc.org) contains supplemental text, Figs. 1–3, Tables 1 and 2, and additional references.

[1] Both authors contributed equally to this work.

[2] To whom correspondence may be addressed. Tel.: 86-27-6875-2831; Fax: 86-27-6875-2146; E-mail: ylwu@whu.edu.cn.

[3] To whom correspondence may be addressed. Tel.: 86-27-8779-2153; Fax: 86-27-8779-2024; E-mail: jpding@mail.hust.edu.cn.

[4] The abbreviations used are: ChTX, charybdotoxin; HEDTA, *N*-hydroxyethylenediaminetriacetic acid; WT, wild type.

At 90% confluence, cells were transiently transfected using Lipofectamine2000 (Invitrogen). Electrophysiological experiments were performed at 1–2 days after transfection.

Solutions—Cells were maintained in ND-96 solution (pH 7.5) containing the following (in mM): 96 NaCl, 2 KCl, 1.8 $CaCl_2$, 1 MgCl, 2.5 sodium pyruvate, and 10 HEPES without penicillin. For inside-out recording, the pipette extracellular solution contained the following (in mM): 160 $MeSO_3K$, 2 $MgCl_2$, 10 HEPES (pH 7.0) titrated with $MeSO_3H$. The intracellular solution contained the following (in mM): 160 $MeSO_3K$, 10 HEPES, 5 HEDTA with added Ca^{2+} to make 10 μM free Ca^{2+}, as defined by the EGTAETC program (McCleskey, Vollum Institute, Portland, OR) at pH 7.0. Zero Ca^{2+} solution contained the following (in mM): 160 $MeSO_3K$, 10 HEPES, 5 EGTA at pH 7.0, titrated by $MeSO_3H$. The ChTX solution was made by adding 100 nM ChTX to the extracellular solution. All chemicals were purchased from Sigma.

Patch Clamp Recording—Patch pipettes were pulled from borosilicate glass capillaries with resistance of 2–4 megohms when filled with pipette solution. An inside-out or outside-out patch was excised from the transfected HEK293 cells. Experiments were performed using a PC2C patch clamp amplifier with corresponding software (InBio, China). Currents typically were digitized at 100 kHz and filtered at 5 kHz.

During recording, the corresponding solutions were perfused locally into cells via a perfusing pipette containing seven solution channels. All experiments were performed at room temperature (22–25 °C).

Data Analysis—Recorded data were analyzed using Clampfit(Axon Instruments, Inc.), Sigmaplot (SPSS, Inc.) software. Unless otherwise stated, the data are presented as mean ± S.E.

The conductance-voltage (*G-V*) curves for activation were generated from steady-state currents, converted to conductance, and then fitted by the single Boltzmann function with the form shown in Equation 1,

$$G/G_{max} = (1 + \exp((V - V_{50})/\kappa))^{-1} \quad \text{(Eq. 1)}$$

where V_{50} is the voltage at which the conductance (G) is half the maximal conductance (G_{max}), and κ is a factor affecting the steepness of the activation. The time courses of onset (or start to block) and offset (or recovery from blockade) were fitted with the first-order blocking reaction, in which the time constants of onset and offset were given by $\tau_{on} = 1/(f\cdot[\text{drug}] + b)$ and $\tau_{off} = 1/b$, where f is the forward drug blocking rate in $M^{-1}\ s^{-1}$, and b is the drug dissociation rate in s^{-1}.

During application of drug (for $t_0 < t \leq t_1$), Equation 2 is achieved,

$$I(t) = (I_0 - I_{ss}) \cdot \exp(-t/\tau_{on}) + I_{ss} \quad \text{(Eq. 2)}$$

During recovery (for $t > t_1$), Equation 3 is achieved,

$$I(t) = I_r - (I_r - I_{ss}) \cdot \exp(-(t - t_1)/\tau_{off}) \quad \text{(Eq. 3)}$$

where I_0 is the mean control current amplitude; I_{SS} is $I_0 \cdot b/(f\cdot[\text{drug}] + b)$ (which indicated a steady-state level of current during blockade by a given drug concentration); I_r is the empirically determined current that is unblocked at the end of the drug application period, $t = 0$ at the time of the drug application, and t_1 is the time of drug washout. The equilibrium dissociation constant (K_d) was defined by $K_d = b/f = [\text{CTX}]/((\tau_{off}/\tau_{on}) - 1)$ (14).

Construction of the mSlo and hβ4 Structure Models—With the exception of the channel turret, the central pore and transmembrane domains of mSlo share strong sequence identity with the structurally determined K^+ channel Kv1.2 (Fig. 1*C*). Based on this, we constructed the closed mSlo structure using three steps. (i) The mSlo turret conformation was obtained through a segment-assembly homology modeling method (15, 16). (ii) The rest of the mSlo structure was directly modeled using the KcsA structure (Protein Data Bank code 1BL8) as a template through the SWISSMODEL server. (iii) These segments were co-assembled into an intact mSlo structure, whose turret is similar to that of the Kv1.2 structure (Protein Data Bank code 2A79) (Fig. 1*D*). Finally, 5-ns unrestrained molecular dynamic simulations were performed with this model to obtain an equilibrated conformation of mSlo.

In this work, only a partial extracellular region (105–137 amino acids) of the hβ4 subunit was selected to predict the possible interaction between mSlo and hβ4 because the selected region is rich in basic residues (Lys-120, Arg-121, and Lys-125), which would be predicted to be the only possible region to bind the acidic residues in the mSlo turret via a salt bridge interaction. Using our previous hERG channel turret as a template (16), the starting hβ4 structure was modeled, and the "qualified" β4 structures were obtained from the dynamic conformation sampling during the 5-ns molecular dynamic simulations of initial model. To obtain a favorable and stable mSlo+hβ4 complex, the selected qualified β4 conformations were placed near the mSlo turret region within a distance of 20 Å, followed by unrestrained 8-ns molecular dynamic simulations to screen for the final reasonable and equilibrated mSlo-hβ4 conformation.

Protein Docking and Molecular Dynamics Simulation—All of the 12 ChTX conformations from NMR (Protein Data Bank code 2CRD) and the modeled mSlo structure were used to improve the rigid docking performance of the molecular mocking algorithm ZDOCK. The following procedures of clustering and screening of reasonable ChTX-mSlo complex structures were similar to our previous work (15, 16).

After stepwise pre-equilibrations (the detailed procedures were the same as described previously (16)), the final ChTX-mSlo and mSlo+β4 complex structures were sufficiently equilibrated by 8-ns molecular dynamic simulations using the Amber 8 program (16) on a 66-CPU Dawning TC4000L cluster (Beijing, China), during which all interaction regions in the complex were totally unrestrained. The ff99 force field (Parm99) (17) was applied throughout the energy minimization and MD simulations.

RESULTS

Open Structural Conformation of the mSlo Turret—It is known that the ChTX blocks BK mSlo channel with an equilibrium dissociation constant K_d of 2–4 nM (4, 7, 18). An estimation of the approximate K_d value for blockade by ChTX can be obtained from two exponential fits of the onset (block) and offset (unblock) time courses (see Equations 2 and 3 in "Exper-

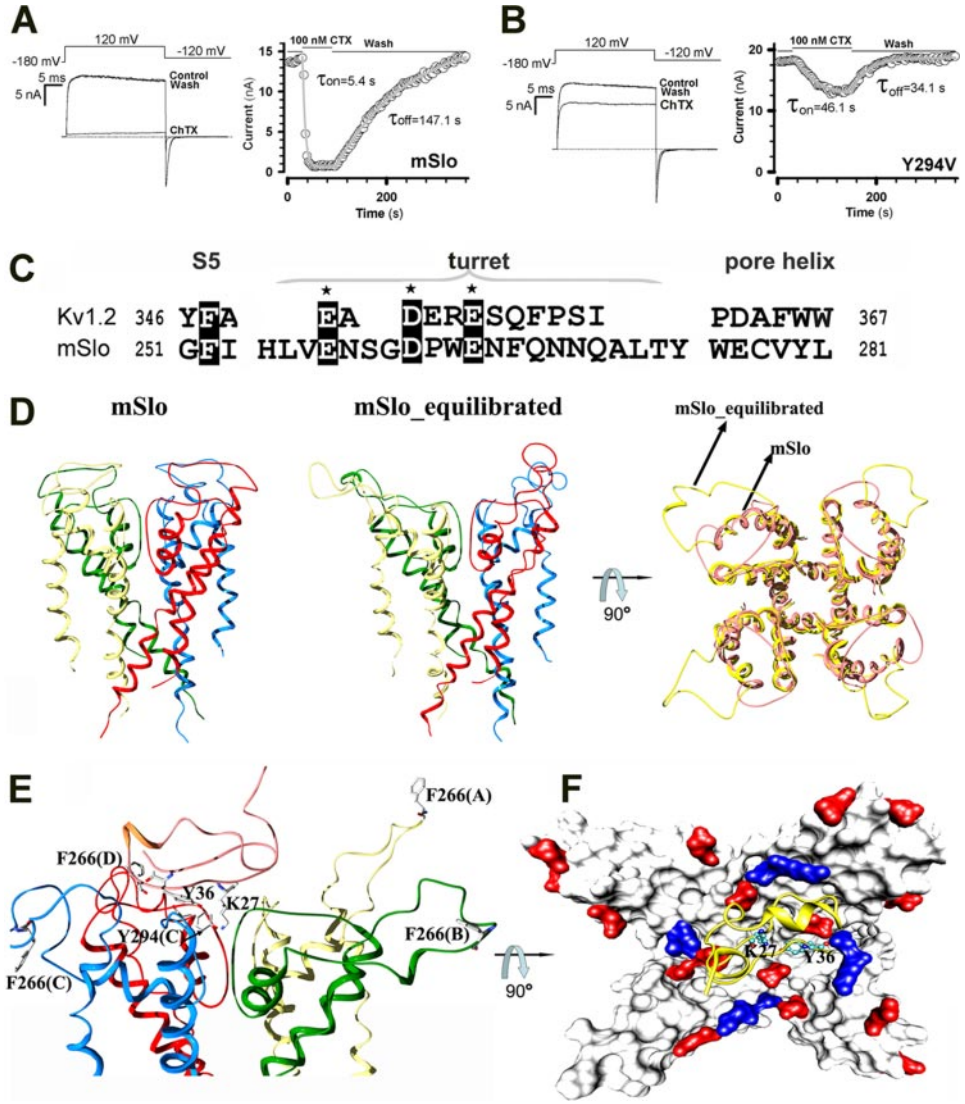

FIGURE 1. **Characteristics of the mSlo channel and the ChTX-mSlo complex.** *A* and *B*, traces shown on the *left panel* were obtained from outside-out patches from HEK293 cells transfected with cDNA encoding mSlo or Y294V subunits. The representative currents were activated by a voltage step from −180 to +120 mV for 30 ms, in the presence and absence of 100 nM ChTX with intracellular 10 μM Ca^{2+}. A voltage protocol is plotted at the *top* of each trace. *Dotted lines* represent zero current. On the *right panel*, the peak currents from the above patches are plotted as a function of elapsed time. Currents were elicited by intracellular 10 μM Ca^{2+} with repetitive voltage steps to +120 mV with a time interval of 3 s, before, during, and after the application of 100 nM ChTX as indicated by the *horizontal bars*. The fractional blocking, activation (τ_a) and deactivation (τ_d) time constants are as follows: 0.90 ± 0.02 (n = 4), 0.90 ± 0.07 and 0.68 ± 0.10 ms (n = 15) for mSlo1; 0.34 ± 0.02 (n = 5), 0.86 ± 0.03, and 0.79 ± 0.05ms (n = 14) for Y294V. The onset (τ_{on}) and the offset (τ_{off}) time constants are as follows: 7.2 ± 1.8 and 106.5 ± 4.7 s (n = 5) for mSlo1; 37.9 ± 2.8 and 37.6 ± 3.4 s (n = 4) for Y294V. *C*, sequence alignment of mSlo with K_V1.2 channels. The *dark shaded letters* are for identical residues. The acidic residues in the turret are marked at the top of the sequence with the *asterisk*. *D*, ribbon views of the starting and equilibrated mSlo structures with their comparison. *E*, overall view of the mSlo-ChTX complex. The putative interaction sites are labeled on both mSlo and ChTX. Four subunits of the tetramer are distinguished by color. *F*, surface representation of the mSlo-ChTX complex with basic residues colored in *blue* and acidic residues in *red*, with ChTX in a schematic structure.

imental Procedures"). With the use of this procedure, 100 nM ChTX blocked the mSlo currents with τ_{on} = 5.4 s and τ_{off} = 147.1s, which conferred a K_d = 3.8 nM (Fig. 1*A*). In the Shaker potassium channel, the residue Thr-449 corresponding to the Tyr-294 (mSlo) was found to be essential for ChTX binding in the linker between the K^+ ion selectivity filter and the S6 transmembrane helix (19). For characterizing the interaction between ChTX and mSlo, the mutant Y294V (mSlo) was selected to investigate the effect on ChTX association. In Fig. 1*B*, 100 nM ChTX induced an ~34% blockade of currents of the mutant Y294V with a slow τ_{on} = 46.1 s and a fast τ_{off} = 34.1 s, suggesting that ChTX has a K_d value for Y294V much larger than that for the wild type mSlo1 because of $\tau_{off}/\tau_{on} \approx 1$ (see "Experimental Procedures"). Therefore, to determine the K_d value of Y294V, we need to increase the ChTX concentration. Alternatively, the recovery time constant (τ_{off}) can be used to estimate the K_d. For instance, a larger τ_{off} corresponds to a higher affinity for the toxin or a lower K_d. Consequently, the fast recovery of Y294V from inhibition implies that the residue Tyr-294 is a critical site for ChTX binding.

Comparison of the sequences between the classical K_V1.2 channel and the mSlo channel revealed a nine amino acid difference in the turret length (Fig. 1*C*). To understand this discrepancy, a computational technique was used to determine the structural conformation of the mSlo turret (15, 16). For the unbound mSlo channel, the starting structure of mSlo was found to be very unstable during the 5-ns molecular dynamic simulations (MDs). The four turrets of the mSlo channel dispersed each other from the pore region (Fig. 1*C*) until equilibrium was reached in the structure. The equilibrated structure of mSlo was used to calculate the structural conformation of mSlo-ChTX complex through docking and 8 ns MDs (Fig. 1, *D* and *E*).

In the mSlo-toxin complex structure, the Tyr-294 residue in the filter S6 linker is located just below Tyr-36 (ChTX) within a contact distance of 4 Å (Fig. 1*D*). Undoubtedly, this is a key residue for the BK channel to bind with ChTX, because the valine substitution of Tyr-294 (Y294V) results in a large loss of sensitivity to ChTX (Fig. 1*B*). In contrast, four Phe-266 residues, residing in the middle of each turret, are located more distally from ChTX (Fig. 1, *C* and *D*). Therefore, these likely will not serve as binding sites, which is consistent with the previous experimental results (20). In conclusion, both the unbound and bound structures of mSlo reveal that it has an open conformation with four dispersive and flexible turrets.

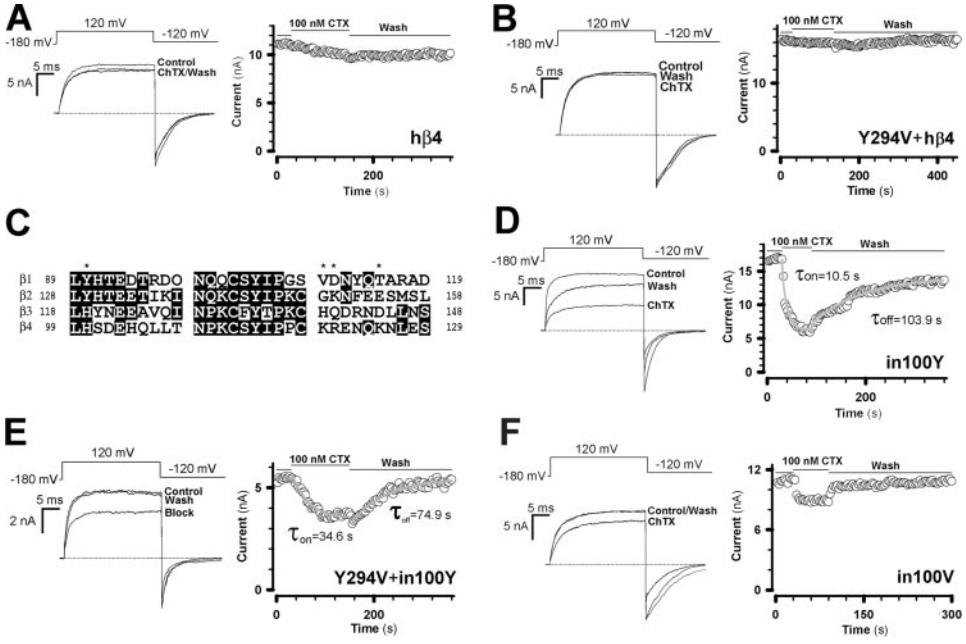

FIGURE 2. **An inserted tyrosine increases the sensitivity of mSlo+hβ4 channels to ChTX.** *A* and *B, traces* shown on the *left* were obtained from outside-out patches from HEK293 cells transfected with cDNA encoding α+hβ4 and Y294V+hβ4 subunits, respectively. The representative currents were activated by a voltage step from −180 to +120 mV for 30 ms, in the presence and absence of 100 nM ChTX with intracellular 10 μM Ca^{2+}. A voltage protocol is plotted at the *top* of each trace. *Dotted lines* represent zero current. On the *right panel*, the peak currents from the above patches are plotted as a function of elapsed time. Currents were elicited by intracellular 10 μM Ca^{2+} with repetitive voltage steps to +120 mV with a time interval of 3 s, before, during, and after the application of 100 nM ChTX as indicated by the *horizontal bars*. The fractional blocking, activation (τ_a), and deactivation (τ_d) time constants are as follows: 0.15 ± 0.02 (n = 4), 2.02 ± 0.10 and 4.50 ± 0.54 ms (n = 17) for mSlo1+β4; 0.08 ± 0.04 (n = 5), 3.90 ± 0.47 and 4.08 ± 0.45ms (n = 12) for Y294V+β4. *C,* sequence alignment for the β subunit family. The *boxed* residues in *dark gray* are the identical residues. The *asterisks* marked at the *top* of the sequence indicate the mutation sites. The in100Y represents a mutant of hβ4 constructed by inserting a tyrosine at position 100. The *letter C3* represents the third conserved cysteine residue in the extracellular region of the β subunit. *D–F, traces* shown on the *left* were obtained from outside-out patches from HEK293 cells transfected with cDNA encoding α+in100Y, Y294V+in100Y, and α+in100V subunits, respectively. The fractional blocking, activation (τ_a) and deactivation (τ_d) time constants are as follows: 0.56 ± 0.09 (n = 5), 1.98 ± 0.13 and 2.98 ± 0.18 ms (n = 15) for α+in100Y; 0.35 ± 0.04 (n = 5), 2.16 ± 0.16 and 3.48 ± 0.35ms (n = 10) for Y294V+in100Y; 0.21 ± 0.07 (n = 4), 3.36 ± 0.31ms and 3.80 ± 0.63ms (n = 14) for α+in100V. The onset (τ_{on}) time constant and the offset (τ_{off}) time constant are as follows: 12.7 ± 2.2 and 126.2 ± 3.1 s (n = 5) for mSlo1+in100Y; 37.9 ± 6.2 and 79.3 ± 8.4s (n = 5) for Y294V+in100Y. Others are the same as described in *A* and *B*.

A Tyrosine Insertion in hβ4 Increases the Channel Sensitivity to ChTX—With the exception of the β1 subunit, BK channels composed of mSlo α and the β2/β3 subunits show 10 times lower sensitivity to ChTX compared with α channels alone (3, 4, 18). Notably, the sensitivity of α+β4 to the scorpion toxins, *e.g.* ChTX, is 1000-fold lower than that of α alone (7, 12). Because the number of β subunits per channel greatly affect the sensitivity to the toxin (1, 21, 22), it is very important to ensure the 1:1 stoichiometry of α+β4 subunits in all β4 experiments. For this purpose, we overexpressed β4 by transfection and then examined the activation and deactivation rates of α+β4 currents to ensure four β4 per channel (see supplemental Fig. 1).

Compared with the currents of α alone channels, we showed that the currents of α+hβ4 channels were reduced by only about 10% in amplitude after a 2-min exposure to 100 nM ChTX (Fig. 2*A*). The on-time course of ChTX blocking the α+hβ4 currents was slow, and the off-time course was much slower, which suggested that ChTX must be confined within a very narrow space. In addition, the Y294V+hβ4 currents showed almost no inhibition in response to 100 nM ChTX compared with about 10% inhibition of the α+β4 currents (Fig. 2*B*), indicating that Tyr-294 of α+hβ4 channels is a binding site that ChTX can only partially access. Furthermore, it may explain the fact that about 20% irreversible inhibition by ChTX often occurs in experiments relevant to the β2 and β3 subunits (4). This likely indicates that a "helmet" formed by both the turret of mSlo and the outer segment of hβ4 seriously impedes the ability of ChTX to approach the residue Tyr-294 (mSlo).

Of the four β subunits, only the β4 subunit is missing the conserved Tyr-100 residue (Fig. 2*C*). Thus, restoration of the missing residue Tyr in β4 might re-establish higher sensitivity to the toxin. In good agreement with our hypothesis, the sensitivity of the α+hβ4 channels to ChTX increased dramatically after inserting Tyr-100 into hβ4 (Fig. 2*D*). The insertion conferred a slower recovery time constant indicating it is the higher affinity of hβ4 to the toxin. In Fig. 2*E*, Y294V+in100Y showed an ~35% inhibition of currents with an onset time constant of τ_{on} = 34.6 s and an offset time constant of τ_{off} = 74.9 s, of which τ_{off} was faster than that of α+in100Y (Fig. 2*D*). The difference between Y294V+in100Y and Y294V is that the former τ_{off} is 2-fold longer than the latter (Fig. 1*B* and Fig. 2*E*), indicating that in100Y has a higher affinity to ChTX than WT β4. The fast on-time course also indicates that Tyr-100 is an easily accessible site for the toxin. To study the function of the introduced Tyr-100, we constructed a β4-mutant (in100V). In Fig. 2*F*, no more than a 20% reduction in the amplitude occurred in α+in100V channels, which was comparable with the 10% reduction in α+β4. Surprisingly, the on-time and off-time courses of α+in100V appeared to be much faster than that of α+β4, indicating that both the on-rate and off-rate of in100V are much faster than that of β4. Therefore, in100V had only low affinity to ChTX, which showed that the inserted aromatic residue tyrosine is a critical binding residue for ChTX. This may explain why in100V only gave a slight reduction in amplitude in response to 100 nM ChTX. In Fig. 2*F*, the slower recovery time course probably resulted from the Tyr-294 with the higher affinity to ChTX, because it also appeared on the off-time course of α+hβ4 (Fig. 2*A*). Therefore, we inferred that Tyr-294 is the binding site for ChTX, and the inserted Tyr-100 is the missing binding site of ChTX.

Basic Residues of the Extracellular Segment of β4 Retard the Inhibition by Toxins—Peptidyl scorpion toxins typically are rich in basic residues. For instance, ChTX has six net positive charges (Fig. 3*A*). One in particular, Lys-27, inserts its positively

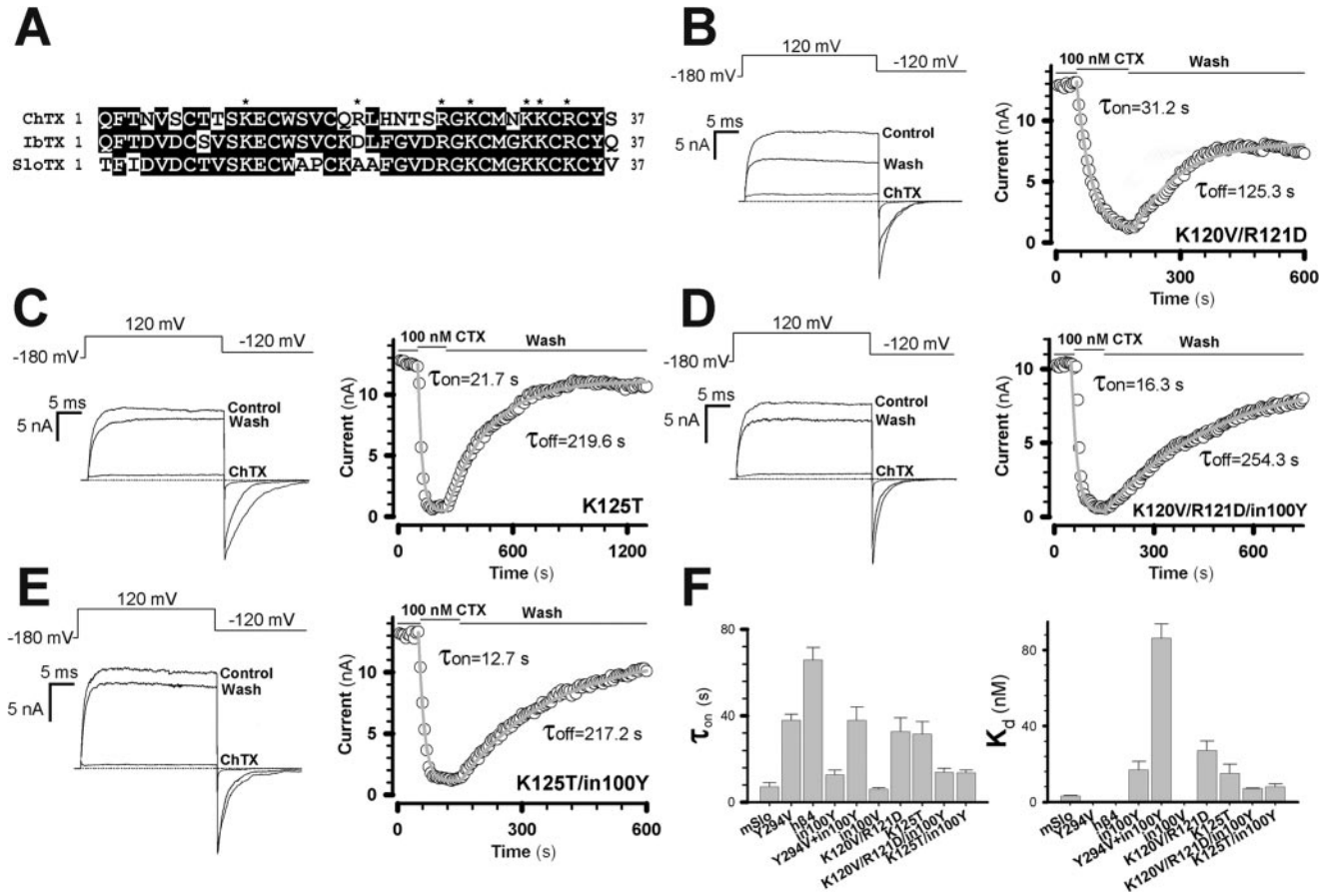

FIGURE 3. **The basic residues of the hβ4 outer segment decrease the sensitivity of mSlo1+hβ4 channels to ChTX.** *A,* sequence alignment for peptidyl scorpion toxins. The *boxed* residues in *dark gray* are the identical residues. The *asterisks* marked at the *top* of sequence indicate basic residues in the peptides. *B–E,* current traces and time courses of blockade on mSlo+K120V/R121D, mSlo+K125T, mSlo+K120V/R121D/in100Y, and mSlo+K125T/in100Y channels are the same as described in Fig. 2, except the time intervals between two repetitive voltage protocols were 10 s for mSlo+K125T and 5 s for others. *Dotted lines* represent the zero current. The fractional blocking, activation (τ_a) and deactivation (τ_d) time constants are as follows: 0.93 ± 0.03 (n = 5), 1.33 ± 0.12 and 2.35 ± 0.29 ms (n = 11) for mSlo+K120V/R121D; 0.95 ± 0.07 (n = 5), 1.58 ± 0.24 and 2.83 ± 0.49 ms (n = 16) for mSlo+K125T; 0.93 ± 0.02 (n = 5), 1.61 ± 0.09 and 3.86 ± 0.85ms (n = 10) for mSlo+K120V/R121D/in100Y; 0.93 ± 0.02 (n = 5), 1.52 ± 0.11 and 3.67 ± 0.62 ms (n = 12) for mSlo+K125T/in100Y. *F,* on the *left panel*, the on-time constants (τ_{on}) of blockade of BK channels were obtained from a single exponential fit to the time courses of reduction on current amplitude as shown in Figs. 2 and 3. Values for τ_{on} are as follows: 7.2 ± 1.8 s (n = 5) for mSlo alone, 37.9 ± 2.8 s (n = 4) for Y294V alone, 65.8 ± 5.7s (n = 4) for mSlo+hβ4, 12.7 ± 2.2 s (n = 5) for mSlo+in100Y, 37.9 ± 6.2 s (n = 5) for Y294V+in100Y, 6.1 ± 0.6 s (n = 4) for mSlo+in100V, 32.8 ± 6.2 s (n = 5) for mSlo+K120V/R121D, 31.6 ± 5.7s (n = 5) for mSlo+K125T, 13.9 ± 1.8s (n = 5) for mSlo+K120V/R121D/in100Y, 13.7 ± 1.2s (n = 5) for mSlo+K125T/in100Y. On the *right panel*, the equilibrium dissociation constants (K_d) for ChTX blockade are only plotted for part of the BK channels as described the above. Values for K_d are as follows: 3.3 ± 0.2 nM (n = 5) for mSlo alone, 16.9 ± 4.4 nM (n = 5) for mSlo+in100Y, 86.4 ± 7.4 nM (n = 5) for Y294V+in100Y, 27.1 ± 5.0 nM (n = 5) for mSlo+K120V/R121D, 15.1 ± 4.9 nM (n = 5) for mSlo+K125T, 7.2 ± 0.1 nM (n = 5) for mSlo+K120V/R121D/in100Y, 8.1 ± 1.4 nM (n = 5) for mSlo+K125T/in100Y.

charged side chain into the outer vestibule to obstruct BK channels (Fig. 1, *E* and *F*) (23–25). The middle region of the β4 subunit contains more basic residues compared with the ChTX-sensitive β1 subunits (Fig. 2*A*). To examine their function, a couple of β4 mutants (K120V/R121D and K125T) were co-expressed with the α subunits. In Fig. 3, *B* and *C*, both α+hβ4 mutant channels exhibited a faster blocking time course, suggesting increased sensitivity to the toxin. Therefore, three basic residues (Lys-120, Arg-121, and Lys1–25) must play an important role in the blockade of ChTX.

Taken together, our results predicted that the double mutations (K120V/R121D/in100Y and K125T/in100y) would show increased sensitivity to ChTX. In line with our hypothesis, the double mutation K125T/in100Y and K120V/R121D/in100Y in fact did accelerate the blocking on-time course to yield a K_d~7 nM, which was about a 2-fold greater K_d for α alone (Fig. 3, *D–F*). In Fig. 3, the results showed a slower recovery time course when all the mutants contained an inserted tyrosine at position 100, suggesting that this is a missing binding site for β4. In conclusion, the restoration of ChTX sensitivity indicates that both the missing Tyr-100 and the basic residues (Lys-120, Arg-121, and Lys-125) make β4 distinctly different from the other β subunits.

In Fig. 4, mutant 4K4D shows greater sensitivity to ChTX than wild type hβ2, suggesting that the electrostatic interaction is a common feature between peptides and mSlo+β channels. In contrast to mutant in100V (hβ4), mutant Y130V (hβ2) showed higher affinity to ChTX, suggesting that Tyr-130 is an important site for binding to the ChTX-hβ2 complex. Interestingly, mutant Y90V (hβ1) showed no effect with respect to ChTX sensitivity compared with hβ1,[5] indicating that the outer

[5] J. Ding, unpublished data.

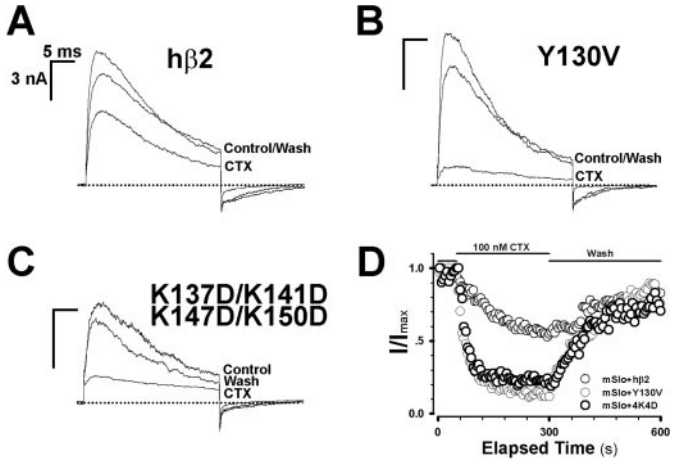

FIGURE 4. **The outer segment of hβ2 affects the sensitivity of mSlo+hβ2 channels to ChTX.** *A–C, traces* show the representative currents obtained from outside-out patches from HEK293 cells transfected with cDNA encoding mouse α+hβ2, α + Y130V, and α + K137D/K141D/K147D/K150D (α + 4K4D) subunits, respectively. Currents were elicited by a 30-ms voltage step from −180 to 120 mV in 10 μM Ca^{2+}. The *lines* represent the control, 100 nM ChTX, and recovery, respectively, as indicated. *D,* each patch was perfused with 100 nM ChTX indicated by the *horizontal bars*. The *circles* are for α+hβ2, α + Y130V, and α + 4K4D, respectively, as indicated.

structural conformation varies across the β family. However, the electrostatic interaction likely becomes the common factor affecting ChTX binding.

Closed Structural Conformation of the mSlo+hβ4 Complex—As mentioned previously, the turrets of the mSlo α subunits form an open conformation in the extracellular pore region. After association with the hβ4 subunits, the extracellular structural conformation of BK channels should have a helmet structure. We inferred that the cluster of three acidic residues (Glu-257, Asp-261, and Glu-264) in the mSlo turret might form a salt bridge with the cluster of three basic residues (Lys-120, Arg-121, and Lys-125) lying in the outer segment of hβ4. Through a series of structural modeling and calculations by 8-ns MDs, the equilibrated structure of the mSlo+hβ4-coil complex was obtained (Fig. 5, *A* and *B*). To investigate the range of conformational movement, we selected the Glu-264 of turret as the reference residue, and we found that the average distance between the two next C-α atoms was about 20 Å (Fig. 5*A*). Therefore, the synergic action of both mSlo and hβ4 subunits via electrical interaction most likely helps to form a helmet with the eight-carbon positively charged ring, which effectively can impede the entry of lysine-rich ChTX with six positive charges

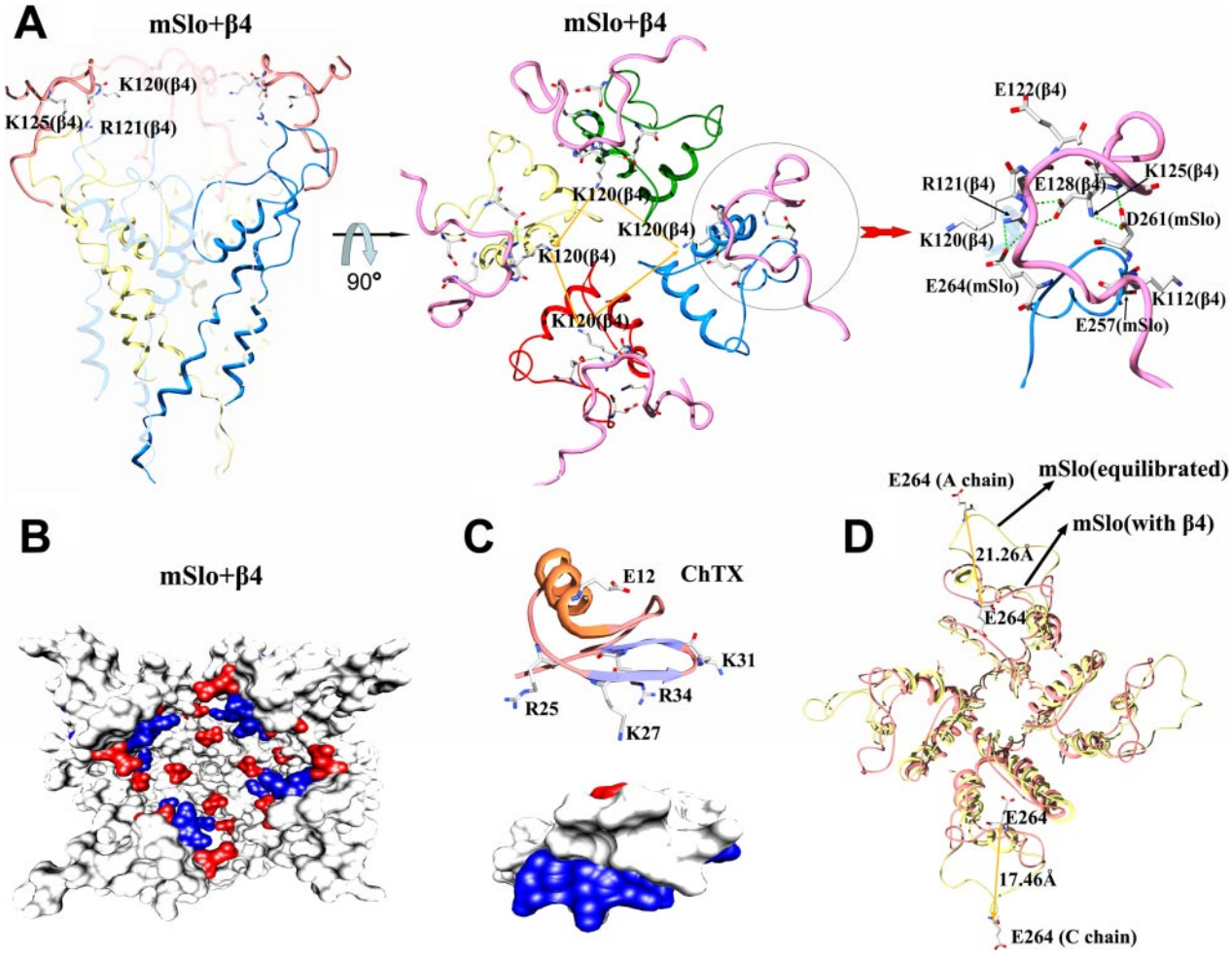

FIGURE 5. **A predicted structural conformation of mSlo+hβ4-coil complex.** *A,* overall view of the equilibrated mSlo+hβ4 complex is shown on the *left panel*. The hβ4 subunits are colored in *pink*. In the *middle panel*, the four Lys-120 of hβ4 are marked by *orange arrowheads* form the helmet of the mSlo+hβ4 complex. The *green line* represents a hydrogen bond between two atoms. The structural details of the mSlo S5P and hβ4-coil are shown on the *right panel*. *B,* surface rendering of the mSlo+hβ4 complex. Basic residues are colored in *blue* and acidic residues in *red*. *C,* views of ChTX in ribbon and molecular surface. *D,* magnitude of the mSlo conformational change induced by hβ4 subunits. Distances are measured from the C-α atoms of the two middle Glu-264 residues in the mSlo turret. Color schemes are the same as described in Fig. 1.

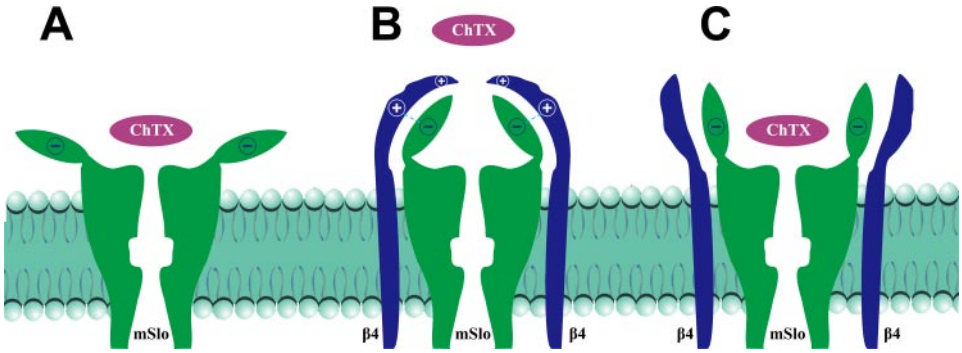

FIGURE 6. **Possible toxin resistance mechanism of the hβ4-associated BK channels.** *A,* ChTX blocking the mSlo tetramer consisting of four turret "scattering petals." *B,* an alabastrum derived from mSlo associated with the hβ4 subunit though an electrostatic interaction that restricted ChTX entry. *C,* when the basic residues in hβ4 were removed, the "flower" of mSlo will "reblossom" to recognize ChTX.

by both electrical repulsion and spatial inhibition (Fig. 5, *C* and *D*). The mutants K120V/R121D and K125T can restore ChTX sensitivity probably by reducing the repulsive force of the electrostatic field and somehow demolishing the elaborate helmet structure. This significant conformational change in the mSlo channel not only reveals that the turret of the mSlo subunits is fully flexible but also suggests that the turret domain plays an essential role in the intrinsic function of the channel. At least the closed structural conformation of mSlo+hβ4 is critical in maintaining the charged helmet for resisting ChTX entry (Fig. 5, *A* and *B*).

DISCUSSION

Of the four β subunit family members, only the brain-enriched hβ4 shows extremely low sensitivity to the toxin. In an effort to explore the mechanism, we had tremendous difficulties because of the lack of structural conformation of hβ4 subunits. With the application of computational and experimental methods, we revealed that a plausible conformational rearrangement of the α+hβ4-coil subunits might lead the channel to resist the binding of ChTX via both electrostatic interaction and limited space.

Fig. 6 shows a schematic used to explain how the ChTX selectively recognizes the mSlo channel in the presence and absence of hβ4 subunit (Fig. 6, *A–C*). The mSlo channel is like a blooming flower with four scattering petals, and the ChTX peptide represents a bee that specifically recognizes the mSlo channel (Fig. 6*A*). When co-expressed with the hβ4 subunit, BK channels will become an alabastrum with four hβ4 subunits acting as peripheral "petals" (Fig. 6*B*). In reality, the structure resembles a helmet maintained by salt bridge interactions. Simultaneously, the positive charges located at the top of α+hβ4 can effectively control the recognition of the lysine-rich ChTX. Removal of those basic residues may fully or partially disassemble the helmet. At this stage, reopening of the turret of the BK channel behaves like a half-blooming flower (Fig. 6*C*).

Compared with the other three β subunits, the hβ4 subunit lacks the tyrosine at position 100 and contains a cluster of basic amino acids within the 120–125-amino acid coil of the hβ4 extracellular region. Thompson and Begenisich (26) reported that protonation of a single amino acid Phe-425 (or F425H) had an unexpectedly large effect on the affinity of the shaker channel for ChTX and inferred that an electrostatic environment near position 425 might be basic in nature. In this study, there are six positive charges along ChTX that interact with approximately eight positive charges in the coil of hβ4. Thus, the electrostatic repulsion at the peptide-channel interface can impede the approach of ChTX to the channel vestibule. In addition, an electrostatic field can change the local concentration of peptides.

In the supplemental material, we show V_{50}, activation (τ_a), and deactivation (τ_d) time constants of WT and its mutants (supplemental Figs. 1–3 and supplemental Table 1). According to V_{50} for 0 or 10 μM Ca^{2+}, τ_a and τ_d for 10 μM Ca^{2+}, all mutants in either mSlo1 or β4 subunit did not show significantly modifications of the apparent calcium-voltage sensitivity as would have been observed with WT β4. In other words, none of the mutants showed significant differences in activation (τ_a) and deactivation (τ_d) time constants compared with mSlo1+β4, except that Y294V+in100V had an acceptable 17.7-mV shift in V_{50}.

The lack of effect of ChTX on β4 likely is because of the presence of the basic residues (Lys-120, Arg-121, and Lys-125) in the β4-loop that impede ChTX entry. For example, both β4 and the mutant K120V/R121D have similar calcium-voltage sensitivities (supplemental Fig. 3 and supplemental Table 1), but the mutant K120V/R121D has a K_d = 27 nM (Fig. 3*B*), indicating that the lack of effect of ChTX is not because of a shift in calcium-voltage sensitivity in the presence of the β4 subunit compared with the α subunit alone. Compared with WT, none of the mutants induced obvious changes in V_{50}, indicating that the α subunits always associated with the β subunits. Therefore, our results, derived from the pharmacological effect of ChTX on those channels, suggested that the residues studied here were important for ChTX binding *per se*.

Our results revealed that both Tyr-294 of the α subunits and the missing Tyr-100 of the β4 subunits are the possible binding sites for ChTX, arising from either a direct association or a binding domain relevant to the residues. Tyr-294 showed higher affinity to the toxin than Tyr-100. Thus, there are two different K_d values possibly appearing in the ChTX inhibition experiments. The lower K_d value comes from Tyr-294, whereas the higher K_d value results from the missing Tyr-100. Notably, the 10–20% "permanent" inhibition mediated by Tyr-294 could be neglected in the experiments involving β2 and β3 subunits.

All β subunits have a large cysteine-rich and highly glycosylated outer segment, which possibly forms a compact structure over the channel vestibule (23). Furthermore, the structural calculation for the bound or unbound state of mSlo (Fig. 1, *F–H*) suggests that the mSlo turret has enough flexibility to interact with β subunits in diverse ways. Thus, removal of cysteine or glycosylation can affect the whole structural conforma-

tion and alter the sensitivity of mSlo+hβ4 channels to the toxin.

Although the incomplete picture of the outer structural conformation of hβ4 prevented us from precisely describing the mechanism of toxin-channel interaction, we still can use the toxin to probe the residues on the outer surface of BK channels to acquire additional structural information via site-direct mutagenesis and computational methods. Through modification of the charged residues of peptides, we can alter the selectivity of toxins to channels, which may accelerate the process of designing specific peptides in the future.

Acknowledgment—We thank Dr. C. L. Lingle for the gift of hβ4 clone.

REFERENCES

1. Knaus, H. G., Garcia-Calvo, M., Kaczorowski, G. J., and Garcia, M. L. (1994) *J. Biol. Chem.* **269,** 3921–3924
2. Knaus, H. G., Folander, K., Garcia-Calvo, M., Garcia, M. L., Kaczorowski, G. J., Smith, M., and Swanson, R. (1994) *J. Biol. Chem.* **269,** 17274–17278
3. Wallner, M., Meera, P., and Toro, L. (1999) *Proc. Natl. Acad. Sci. U. S. A.* **96,** 4137–4142
4. Xia, X. M., Ding, J. P., and Lingle, C. J. (1999) *J. Neurosci.* **19,** 5255–5264
5. Xia, X. M., Ding, J. P., Zeng, X. H., Duan, K. L., and Lingle, C. J. (2000) *J. Neurosci.* **20,** 4890–4903
6. Brenner, R., Perez, G. J., Bonev, A. D., Eckman, D. M., Kosek, J. C., Wiler, S. W., Patterson, A. J., Nelson, M. T., and Aldrich, R. W. (2000) *Nature* **407,** 870–876
7. Meera, P., Wallner, M., and Toro, L. (2000) *Proc. Natl. Acad. Sci. U. S. A.* **97,** 5562–5567
8. Uebele, V. N., Lagrutta, A., Wade, T., Figueroa, D. J., Liu, Y., McKenna, E., Austin, C. P., Bennett, P. B., and Swanson, R. (2000) *J. Biol. Chem.* **275,** 23211–23218
9. Weiger, T. M., Holmqvist, M. H., Levitan, I. B., Clark, F. T., Sprague, S., Huang, W. J., Ge, P., Wang, C., Lawson, D., Jurman, M. E., Glucksmann, M. A., Silos-Santiago, I., DiStefano, P. S., and Curtis, R. (2000) *J. Neurosci.* **20,** 3563–3570
10. Brenner, R., Jegla, T. J., Wickenden, A., Liu, Y., and Aldrich, R. W. (2000) *J. Biol. Chem.* **275,** 6453–6461
11. Brenner, R., Chen, Q. H., Vilaythong, A., Toney, G. M., Noebels, J. L., and Aldrich, R. W. (2005) *Nat. Neurosci.* **8,** 1752–1759
12. Jin, P., Weiger, T. M., and Levitan, I. B. (2002) *J. Biol. Chem.* **277,** 43724–43729
13. Zeng, X. H., Xia, X. M., and Lingle, C. J. (2003) *Nat. Struct. Biol.* **10,** 448–454
14. Saito, M., Nelson, C., Salkoff, L., and Lingle, C. J. (1997) *J. Biol. Chem.* **272,** 11710–11717
15. Yi, H., Qiu, S., Cao, Z., Wu, Y., and Li, W. (2008) *Proteins* **70,** 844–854
16. Yi, H., Cao, Z., Yin, S., Dai, C., Wu, Y., and Li, W. (2007) *J. Proteome Res.* **6,** 611–620
17. Wang, J., Cieplak, P., and Kollman, P. A. (2000) *J. Comput. Chem.* **21,** 1049–1074
18. Hanner, M., Schmalhofer, W. A., Munujos, P., Knaus, H. G., Kaczorowski, G. J., and Garcia, M. L. (1997) *Proc. Natl. Acad. Sci. U. S. A.* **94,** 2853–2858
19. Naranjo, D., and Miller, C. (1996) *Neuron* **16,** 123–130
20. Yao, J., Li, H., Gan, G. L., Wu, Y., and Ding, J. P. (2006) *Acta Pharmacol. Sin.* **27,** 945–949
21. Ding, J. P., Li, Z. W., and Lingle, C. J. (1998) *Biophys. J.* **74,** 268–289
22. Wang, Y. W., Ding, J. P., Xia, X. M., and Lingle, C. J. (2002) *J. Neurosci.* **22,** 1550–1561
23. Gao, Y. D., and Garcia, M. L. (2003) *Proteins* **52,** 146–154
24. Park, C. S., and Miller, C. (1992) *Neuron* **9,** 307–313
25. Park, C. S., and Miller, C. (1992) *Biochemistry* **31,** 7749–7755
26. Thompson, J., and Begenisich, T. (2000) *Biophys. J.* **78,** 2382–2391